

Tests for Standard Accretion Disk Models by Variability in Active Galactic Nuclei

H. T. Liu¹, J. M. Bai¹, X. H. Zhao¹, and L. Ma²

ABSTRACT

In this paper, standard accretion disk models of AGNs are tested using light curves of 26 objects well observed for reverberation mapping. Time scales of variations are estimated by the most common definition of the variability time scale and the zero-crossing time of the autocorrelation function of the optical light curves for each source. The measured time scales of variations by the two methods are consistent with each other. If the typical value of the viscosity parameter $\alpha \sim 0.1$ is adopted, the measured optical variability time scales are most close to the thermal time scales of the standard disks. If α is allowed to range from ~ 0.03 to ~ 0.2 , the measured time scales are consistent with the thermal time scales of the standard disks. There is a linear relation between the measured variability time scales and black hole masses, and this linear relation is qualitatively consistent with expectation of the standard accretion disk models. The time lags measured by the ZDCF between different bands are on the order of days. The measured time lags of NGC 4151 and NGC 7469 are marginally consistent with the time lags estimated in the case of continuum thermal reprocessing for the standard accretion disk models. However, the measured time lags of NGC 5548 and Fairall 9 are unlikely to be the case of continuum thermal reprocessing. Our results are unlikely to be inconsistent with or are likely to be conditionally in favor of the standard accretion disk models of AGNs.

Subject headings: accretion, accretion disks — black hole physics — galaxy: active — galaxy: quasars — galaxy: Seyfert

¹National Astronomical Observatories/Yunnan Observatory, the Chinese Academy of Sciences, Kunming, Yunnan 650011, China; liuhongtao1111@hotmail.com; baijinming@ynao.ac.cn.

²Physics Department, Yunnan Normal University, Kunming 650092, China.
send offprint requests to H. T. Liu

1. INTRODUCTION

Large flux variations on time scales from years to hours are common in active galactic nuclei (AGNs), and longer time scale variations of the order of months to years may be related to the propagation of the shorter time scale variations (e.g., Ulrich et al. 1997). The combination of high flux variability and short variability time scales implies that the energy conversion in AGNs is more efficient than the ordinary stellar processes. Accretion of matter onto a black hole can have high energy release efficiency (Rees et al. 1982; Rees 1984). The evidence that AGNs such as quasars and Seyfert galaxies are powered by gravitational accretion of matter onto supermassive black holes is now quite convincing. Certainly there has been no definitive detection of the relativistic effects that would be required for unambiguous identification of a singularity, although studies of the iron $K\alpha$ emission line in the X-ray spectra of AGNs currently provides some promise (e.g., Reynolds & Nowak 2003).

In general optical–UV radiations of most non-blazar type sources are within the so-called Big Blue Bump. The optical variability is characterized as poorly understood, but is nevertheless recognized as a means of probing physical scales that cannot be resolved spatially by any telescope or instrument (e.g., Netzer & Peterson 1997; Peterson et al. 2004; Wold et al. 2007). A number of models have been proposed to explain optical–UV quasar variability. One way of attempting to help constraining the proposed models is to find relationships between variability and other parameters of AGNs, such as black hole mass. The black hole mass is a fundamental parameter of AGNs, and the discovery of such a relationship – or lack thereof – may provide useful clues to the physical mechanisms behind the variability (e.g., Wold et al. 2007). Processes intrinsic to the central engine itself could dominate. Wold et al. (2007) investigate the dependence of quasar variability on black hole mass, and find that black hole mass correlates with the measured variability amplitude. A number of models for quasar optical variability exist but there are no clear predictions relating black hole mass and variability amplitude. Different sources of optical variations can be associated with different characteristic time scales, and many of these time scales depend on black hole mass. Collier & Peterson (2001) attempt to define a relationship between black hole mass and characteristic variability time scale. Studying 10 well-monitored AGNs, they report evidence of black hole mass correlating with characteristic optical variability time scales that are roughly consistent with accretion disk thermal time scales.

The standard accretion disk is the basic model for a radiatively efficient, geometrically thin, optically thick disk (Shakura & Sunyaev 1973). In the standard picture this accretion disk radiates thermally mainly in the optical/UV bands for AGNs with black hole masses of $\sim 10^6$ – $10^9 M_\odot$. AGNs with black hole masses of $\sim 10^7$ – $10^9 M_\odot$ would be expected to have accretion disk thermal characteristic time scales of the order of months to years. Many

investigations based on central radiations from thin accretion disks have been done (e.g., Ebisawa et al. 1991; Hanawa 1989; Li et al. 2005; Pereyra et al. 2006; Zimmerman et al. 2005). Connections of jets and disks, a very important aspect of AGN researches, have been investigated on the basis of standard accretion disks (e.g., Meier 2001, 2002). Though many investigations are on the basis of standard disks, only a few investigations aim at testing standard accretion disk models by observations. Collier et al. (1998) briefly discussed the relation of time delays between the UV and optical continuum variations with accretion disk in NGC 7469. It is believed for non-blazar type AGNs that the optical/UV emissions are produced thermally from accretion disks. The radiation energies of thermal emissions emitted in accretion disks are from two possible contributions. One well-known origin is the local viscous dissipation in accretion disks. This local viscous dissipation can produce the local thermal equilibrium, and then the local blackbody emissions (e.g., Krolik 1999). Another origin is the reprocessed X-rays. The X-rays are commonly attributed to Compton up-scattering of the thermal UV photons produced by the viscous dissipation (e.g., Sunyaev & Titarchuk 1980; Haardt & Maraschi 1991). In the case of thermal emissions from viscous dissipation, the accretion flow fluctuations travelling inwards across the emitting regions affect first the optical emitting region at outer radii, and then the UV emitting region at inner radii. Then the longer wavelength variations are likely to lead the shorter wavelength ones. If the radial temperature profiles of accretion disks are not set primarily by viscous effects, but by irradiation from the central X-ray sources, the longer wavelength variations are likely to lag the shorter wavelength ones for thermal emissions from continuum thermal reprocessing. The flux variability must occur on a physical time scale that is consistent with the chosen model. The time scales of interest are the light crossing, dynamical, thermal, and sound crossing time scales that are set by the black hole mass (Frank, King, & Raine 2002), and the order-of-magnitude scales are

$$\tau_1 = 6M_8\xi_3 \text{ days}, \quad (1)$$

$$\tau_{\text{dyn}} = 6M_8\xi_3^{3/2} \text{ months}, \quad (2)$$

$$\tau_{\text{th}} = \tau_{\text{dyn}}/\alpha = 5M_8\xi_3^{3/2} \text{ yrs}, \quad (3)$$

$$\tau_s = 70M_8\xi_3T_5^{-1/2} \text{ yrs}, \quad (4)$$

where $M_8 = M_{\text{BH}}/10^8 M_\odot$, α (~ 0.1) is the Shakura-Sunyaev viscosity parameter (Shakura & Sunyaev 1973), $T_5 = T/10^5 \text{ K}$, and $\xi_3 = r_d/10^3 r_g$ (r_d is the disk radius, and $r_g = GM_{\text{BH}}/c^2$ the gravitational radius). In order to determine which physical mechanism is responsible for the variability and to test standard accretion disk models, it is necessary to connect the observed variability time scales with one of the above physical time scales and to search the correlation of black hole masses with characteristic optical variability time scales, and it is

important to compare the observed time lags between different bands with the theoretical values predicted by the standard accretion disk models.

The structure of this paper is as follows. The sample and data are in § 2. The calculations of temperature profiles are described in § 3. § 4 presents variability time scales and time lags. § 4.1 is analysis of variability time scale, § 4.2 analysis of time lag, and § 4.3 comparison to models. The last section is discussions and conclusions. Throughout this paper, we use a flat cosmology with a deceleration factor $q_0 = 0.5$ and a Hubble constant $H_0 = 75 \text{ km s}^{-1} \text{ Mpc}^{-1}$.

2. THE SAMPLE AND DATA

The objects listed in Table 1 are based on the samples analyzed by Kaspi et al. (2000) and Peterson et al. (2004), but the light curve data comes from a variety of sources. The rest frame wavelengths and references of light curves are listed in columns (3) and (4) of Table 1, respectively. The optical variability time scales are estimated by the light curves around 5100 \AA . There are four objects, Fairall 9, NGC 4151, NGC 5548, and NGC 7469, that have multi-wavelength light curves well observed at the optical/UV bands. The multi-wavelength light curves are used to estimate time lags for the four objects.

The black hole masses for AGNs have been well estimated by the reverberation mapping technique (e.g., Kaspi et al. 2000, 2005; Peterson et al. 2004, 2005; Vestergaard & Peterson 2006). The masses of the central black holes of quasars span a large range of $10^7 M_\odot \lesssim M_{\text{BH}} \lesssim 3 \times 10^9 M_\odot$, and have an upper limit of $M_{\text{BH}} < 10^{10} M_\odot$ (McLure & Dunlop 2004; Vestergaard 2004). The black hole masses used in this paper are taken from Peterson et al. (2004), and are listed in column (5) of Table 1. The bolometric luminosity L_{bol} of objects except for Mrk 279 are taken from Woo & Urry (2002), and are listed in column (6) of Table 1. The bolometric luminosity of Mrk 279 is estimated by $L_{\text{bol}} \approx 9\lambda L_\lambda(5100 \text{ \AA})$ (Kaspi et al. 2000), with $\lambda L_\lambda(5100 \text{ \AA})$ taken from Peterson et al. (2004).

3. CALCULATIONS OF TEMPERATURE PROFILES

The local effective temperatures of accretion disks are functions of radii r_d , black hole mass M_{BH} , spin a_* , and mass accretion rate \dot{M} (e.g., Ebisawa et al. 1991; Hanawa 1989; Kubota et al. 2005; Li et al. 2005; Pereyra et al. 2006; Shakura & Sunyaev 1973; Zimmerman et al. 2005). The standard accretion disk is the basic model for a radiatively efficient, geometrically thin disk. If the central black holes are Kerr ones, the local effective

temperature of the standard disk is given in the Kerr metric as (Krolik 1999)

$$T_{\text{eff}}(X_d) = \left[\frac{3GM_{\text{BH}}\dot{M}}{8\pi\sigma_{\text{SB}}r_g^3X_d^3} R_{\text{R}}(X_d) \right]^{1/4}, \quad (5)$$

where σ_{SB} is the Stefan-Boltzmann constant, G is the gravitational constant, \dot{M} is the mass accretion rate of the central black hole, M_{BH} is the central black hole mass, and $X_d = r_d/r_g$ is the disk radius in units of the gravitational radius r_g . The function $R_{\text{R}}(X_d)$ in equation (5) is defined as

$$R_{\text{R}}(X_d) = \frac{C(X_d)}{B(X_d)}, \quad (6)$$

where the functions $B(X_d)$ and $C(X_d)$ are, respectively, (Krolik 1999)

$$B(X_d) = 1 - \frac{3}{X_d} + \frac{2a_*}{X_d^{3/2}}, \quad (7)$$

and

$$\begin{aligned} C(X_d) = & 1 - \frac{y_{\text{ms}}}{y} - \frac{3a_*}{2y} \ln \left(\frac{y}{y_{\text{ms}}} \right) \\ & - \frac{3(y_1 - a_*)^2}{yy_1(y_1 - y_2)(y_1 - y_3)} \ln \left(\frac{y - y_1}{y_{\text{ms}} - y_1} \right) \\ & - \frac{3(y_2 - a_*)^2}{yy_2(y_2 - y_1)(y_2 - y_3)} \ln \left(\frac{y - y_2}{y_{\text{ms}} - y_2} \right) \\ & - \frac{3(y_3 - a_*)^2}{yy_3(y_3 - y_1)(y_3 - y_2)} \ln \left(\frac{y - y_3}{y_{\text{ms}} - y_3} \right), \end{aligned} \quad (8)$$

where $y = \sqrt{X_d}$, $a_* = cJ/GM_{\text{BH}}^2$ is the dimensionless spin parameter of the central black hole with the spin angular momentum J , $y_{\text{ms}} = \sqrt{X_{\text{ms}}}$ is the value of y at the marginally stable orbit, and $y_{1,2,3}$ are the three roots of $y^3 - 3y + 2a_* = 0$, respectively (e.g., Krolik 1999; Reynolds & Nowak 2003).

Assuming prograde orbits, the radii of the marginally stable orbits in the equatorial plane of a Kerr black hole are (Bardeen et al. 1972)

$$X_{\text{ms}} = 3 + Z_2 - [(3 - Z_1)(3 + Z_1 + 2Z_2)]^{1/2}, \quad (9)$$

where

$$Z_1 = 1 + (1 - a_*^2)^{1/3} \left[(1 + a_*)^{1/3} + (1 - a_*)^{1/3} \right], \quad (10)$$

and

$$Z_2 = (3a_*^2 + Z_1^2)^{1/2}. \quad (11)$$

The marginally stable orbits in the equatorial plane correspond to the maximum efficiency of energy release as a result of accretion, assuming prograde orbits (Kembhavi & Narlika 1999)

$$\eta_{\max} = 1 - \frac{X_{\text{ms}} - 2 + a_* X_{\text{ms}}^{-1/2}}{\sqrt{X_{\text{ms}} (X_{\text{ms}} - 3 + 2a_* X_{\text{ms}}^{-1/2})}}. \quad (12)$$

According to the definition of the efficiency η with which various types of black holes convert rest mass-energy into outgoing radiation (Thorne 1974), the mass accretion rate of the central black hole can be estimated by the formula

$$\dot{M} = \frac{L_{\text{bol}}}{\eta_{\max} c^2}. \quad (13)$$

The dimensionless spin parameter of a black hole can take on any value in the range $-1 \leq a_* \leq 1$, where negative values of a_* correspond to a black hole that retrogrades relative to its accretion disk. For simplicity we consider only prograde spins up to the Thorne spin equilibrium limit, i.e. $0 \leq a_* \leq 0.998$ (Thorne 1974). The limiting value of $a_* = 0.998$ for black hole spins was first discussed in Thorne (1974). Recent work on magnetohydrodynamic accretion disks suggest a rather lower equilibrium spin (e.g., Gammie et al. 2004; Krolik et al. 2005). It is suggested that spin equilibrium is reached at $a_* \approx 0.93$ through accretion of gases onto the central black holes, and mergers of black holes with comparable mass can result in a final spin of $a_* \sim 0.8\text{--}0.9$ (Gammie et al. 2004). Krolik et al. (2005) suggested that equilibrium spins as low as $a_* \sim 0.9$ are within the realm of possibility. Brenneman & Reynolds (2006) obtained a formal constraint on the dimensionless black hole spin parameter of $a_* = 0.989_{-0.002}^{+0.009}$ at 90% confidence for the Seyfert galaxy MCG–06–30–15. A value of $a_* = 0.9939_{-0.0074}^{+0.0026}$ for the Galactic Center black hole is obtained by Aschenbach et al. (2004). Considering the probable ranges of spin parameter a_* suggested above, we take four values of spin parameter $a_* = 0.5, 0.8, 0.9,$ and 0.998 in the Kerr metric to calculate the temperature profiles. Combining equations (5)–(13) and the parameters of $M_{\text{BH}}, L_{\text{bol}},$ and a_* , we can calculate the surface effective temperature profiles.

The local effective temperature in equation (5) is arrived by assuming local thermal equilibrium (LTE) in disk. A consequence of the LTE radiation assumption is that specific photon frequency ν maps to specific radius r_ν in the disk. According to discussion of Krolik (1999, see equation (7.53) in page 155), most of the light at frequency ν is emitted near the radius r_ν for the local blackbody. Then the optical spectrum may still be dominated by emission from the outer radii, and the UV spectrum can be dominated by emission from the inner radii. So variations in the outer disk might manifest themselves significantly in the observed spectrum.

4. VARIABILITY TIME SCALE AND TIME LAG

Two methods are applied to analysis of variability time scale. One is the most common definition of the variability time scale (e.g., Wagner & Witzel 1995). Another is a well defined quantity, the zero-crossing time of the autocorrelation function of light curves. Time lags are analyzed by the z-transformed discrete correlation function (ZDCF; Alexander 1997). Then the analysis results are compared to predications of accretion disk models.

4.1. Analysis of Variability Time Scale

The variability time scales have been defined in different ways. The most common definition of the variability time scale $\tau = F/|\Delta F/\Delta t|$ and the more conservative approach of $\tau = |\Delta t/\Delta \ln F|$ have the advantage of weighting fluctuations by their amplitudes, where F is the flux, and ΔF is the variability amplitude in the time scale Δt (e.g., Wagner & Witzel 1995). Here we use the most common definition of variability time scale $\tau = F/|\Delta F/\Delta t|$, where F is taken as the flux at the minimum. In this paper, we refer to the interval between subsequent local minima and maxima at the adjacent valleys and peaks in the entire light curve. First, we select subsequent valley and peak sufficiently dense sampled in one light curve. Second, variations of $\Delta F/F \geq 30\%$ between the subsequent minimum and maximum are required within the time scale Δt . The estimated values of τ are listed in column (2) of Table 2. The uncertainty on the values of τ are estimated by the relation $\sigma_\tau = \Delta t(\sigma_{F_{\min}}|\Delta F| - F_{\min}|\sigma_{F_{\max}} - \sigma_{F_{\min}}|)/|\Delta F|^2$, where $\Delta F = F_{\max} - F_{\min}$, $\sigma_{F_{\max}}$ is the observed error of F_{\max} , and $\sigma_{F_{\min}}$ is the observed error of F_{\min} .

For most AGNs, it is difficult to define a single characteristic variability time scale. One approach to a single time scale is described by Giveon et al. (1999). Their definition is given as the zero-crossing time of the autocorrelation function (ACF). If there is an underlying signal with a typical variability time scale in the light curve, the width of the ACF peak near zero time lag will be proportional to this variability time scale (e.g., Giveon et al. 1999; Netzer et al. 1996). This zero-crossing time of the ACF, τ_0 , is a well defined quantity, and is used as a characteristic variability time scale (e.g., Alexander 1997; Giveon et al. 1999; Netzer et al. 1996). Another function used in variability studies to estimate the variability time scale is the first-order structure function (SF) (e.g., Trevese et al. 1994). There is a simple relation between the ACF and the SF (see Eq. (8) in Giveon et al. 1999). Therefore only an ACF analysis is performed on our light curves. Comparison of τ with τ_0 is performed to test the reliability of the variability time scale τ listed in column (2) of Table 2. The ACF is estimated by the ZDCF (Alexander 1997). It has been shown that this method is statistically robust even when applied to very sparsely and irregularly sampled light curves (Alexander

1997). The ZDCF was calculated for all of the light curves used to estimate τ . Following Giveon et al. (1999), a least-squares procedure is used to fit a fifth-order polynomial to the ZDCF, and the ZDCF fit is used to evaluate the zero-crossing time in the observer’s frame.

The evaluated results are listed in column (3) of Table 2. For one light curve, the ZDCF code of Alexander (1997) can automatically set how many bins are given and used to calculate the ACF. Thus, the time lag and its uncertainty are immediately given for each bin in the ACF. However, this code cannot estimate the uncertainty on the fit value of τ_0 to the ACF. If the fit τ_0 is most near the time lag of one bin in the ACF, the uncertainty of the fit τ_0 may be approximated by the uncertainty of time lag in this bin in the ACF. Thus, the uncertainty on the values of τ_0 in Table 2 is assumed to be the errors of the ACF points nearest to the fit values of τ_0 .

For comparison, we plotted τ versus τ_0 in Figure 1. It can be seen in Figure 1 that the data points are basically shared by two sides of the line $\tau_0 = \tau$. The linear regression analysis shows that there is a correlation between τ and τ_0 with Pearson correlation coefficient $r = 0.766$ at the chance probability $P = 5.1 \times 10^{-6}$. The regression line fitted by the ordinary least-squares bisector regression analysis (Isobe et al. 1990) is

$$\tau_0/(1+z) = -96.1(\pm 33.8) + 1.5(\pm 0.3)\tau/(1+z), \quad (14)$$

where z is the redshift, and τ and τ_0 are in units of days. This suggests that the τ and τ_0 are acceptable to characterize the typical variability time scale, and that the estimated results of τ listed in column (2) of Table 2 are reliable.

4.2. Analysis of Time Lag

Cross-correlation function (CCF) analysis is a standard technique in time series analysis to find time lags between light curves at different wavelengths, and the definition of the CCF assumes that the light curves are uniformly sampled. However, in most cases the sampling is not uniform. The interpolated cross-correlation function (ICCF) method of Gaskell & Peterson (1987) uses a linear interpolation scheme to determine the missing data in the light curves. On the other hand, the discrete correlation function (DCF; Edelson & Krolik 1988) can utilize a binning scheme to approximate the missing data. Apart from the ICCF and DCF, there is another method of estimating the CCF in the case of non-uniformly sampled light curves, that is, the z-transformed discrete correlation function (Alexander 1997). The ZDCF was used as an estimation of the ACF in §4.1; here it is used as an estimation of the CCF. The ZDCF is a binning type of method as an improvement of the DCF technique, but has a notable feature that the data are binned by equal population rather than equal

bin width $\Delta\tau$ as in the DCF. It has been shown in practice that the calculation of the ZDCF is more robust than the ICCF and the DCF when applied to sparsely and unequally sampled light curves (e.g., Edelson et al. 1996; Giveon 1999; Roy et al. 2000). The ZDCF is calculated in this paper.

In general, it seems to be true that the time lag is better characterized by the centroid τ_{cent} of the DCF and the ICCF rather than by the peak τ_{peak} , namely, the time lag where the linear correlation coefficient has its maximum value r_{max} (e.g., Peterson et al. 2004, 2005). τ_{peak} is much less stable than τ_{cent} in both the DCF and the ICCF, and τ_{peak} is much less stable in the DCF than in the ICCF (Peterson et al. 2005). Then we prefer that the time lag estimated from the ZDCF method is characterized by the centroid τ_{cent} of the ZDCF, for the ZDCF is an improvement of the DCF method. The centroid time lags τ_{cent} are computed using all points with correlation coefficients $r \geq 0.8r_{\text{max}}$, and the uncertainties for time lags of data points in the ZDCF are computed with a large number (1,000) of Monte Carlo realizations. The ZDCFs of four objects are presented in Figures 2–5, and the measured time lags are listed in column (4) of Table 3.

4.3. Comparison to Models

There is a correlation between the black hole mass M_8 and the measured characteristic variability time scale τ with Pearson correlation coefficient $r = 0.760$ at the chance probability $P = 6.6 \times 10^{-6}$ (see Fig. 6). The regression lines fitted by the bisector regression analysis are

$$\tau/(1+z) = 0.27(\pm 0.04) + 0.12(\pm 0.02)M_8 \text{ yrs.} \quad (15)$$

If $r_d \sim 100 r_g$ in equation (3) with viscosity parameter $\alpha = 0.1$, there is a relation of $\tau_{\text{th}} \sim 0.15M_8$. Though the intercept in equation (15) differs from the intercept predicted by equation (3), this predicted slope of ~ 0.15 is consistent with the one in equation (15). This indicates that the linear correlation between black hole mass and characteristic variability time scale is qualitatively consistent with the expectation of equation (3) that the thermal time scale is essentially linearly related with the black hole mass. Thus, equation (15) is qualitatively consistent with expectations of the standard accretion disk models.

According to the standard accretion disk models, the optical/UV emissions are produced thermally in accretion disks. The standard accretion disk models are used to estimate the radii of maximum optical/UV emissions. We consider accretion disk to be composed of rings with approximately uniform temperature radiating locally as blackbody, and estimate the radii of maximum flux emission at different wavelengths using a disk radial temperature profile given by equation (5). Then the light crossing, dynamical, thermal, and sound crossing

time scales are estimated by equations (1)–(4), respectively, assuming viscosity parameter $\alpha = 0.1$. The calculated results are presented in columns (4)–(7) of Table 2, respectively. It can be seen from columns (2)–(7) of Table 2 that the thermal time scales are most close to the optical variability time scales among the four physical time scales, but the light crossing and dynamical time scales are much smaller than the measured time scales of optical variations, and the sound crossing time scales are much larger than the measured time scales. This might indicate that the optical variations result from the thermal instability in accretion disks or one mechanism related to it. Though, it cannot be affirmed that the optical variations result from the accretion disk thermal instability, the linear relation presented in equation (15) is qualitatively consistent with expectation of equation (3) that the thermal time scale is essentially linearly related with the black hole mass. These above results are obtained by adopting the viscosity parameter $\alpha = 0.1$ for each source in our sample. In practice, various values of α are suggested and used in investigations (e.g., Afshordi & Paczynski 2003; Khajenabi & Shadmehri 2007; Merloni 2003; Merloni & Nayakshin 2006; Pariev et al. 2003). If the viscosity parameter α is allowed to range from $\alpha \sim 0.03$ to $\alpha \sim 0.2$ (e.g., Afshordi & Paczynski 2003), calculations show that the combinations of $\alpha \sim 0.03$ – 0.2 and $a_* = 0.5$ – 0.998 can result in the thermal time scales that are in well agreement with the optical variability time scales presented in Table 2. Then it is likely that the optical variations result from the accretion disk thermal instability.

The radiation energies emitted in accretion disks are probably from the continuum thermal reprocessing and/or the local viscosity dissipation (e.g., Ulrich et al. 1997). If the X-rays illuminating optically thick material in thin disk produce the optical–UV emissions through thermal reprocessing, the optical and UV variations following the X-ray variations are probably correlated with the UV variations leading the optical ones. The time lags in the case of continuum thermal reprocessing are estimated for the standard accretion disks with black hole spin parameter $a_* = 0.5, 0.8, 0.9,$ and 0.998 . The relevant time lags are listed in column (5) of Table 3. The plus signs of values in column (5) mean that the variations at longer wavelengths lag the variations at shorter wavelengths. It can be seen from columns (4) and (5) of Table 3 that the measured time lags are marginally consistent with those predicted by the standard accretion disks for NGC 4151 and NGC 7469. This implies that the optical and UV emissions are likely to be the reprocessed X-rays for NGC 4151 and NGC 7469. In addition, the time lags decrease slightly as spin parameter a_* increases. For Fairall 9 and NGC 5548, the signs of the continuum thermal reprocessing time lags are contrary to those of the measured time lags. This indicates that the optical/UV emissions are unlikely to be the reprocessed X-rays for Fairall 9 and NGC 5548. If variations in the accretion flow affect first the flux at outer radii, and then in the inner region, this maybe result in correlated optical/UV light curves with longer wavelength variations leading shorter

wavelength variations. As a reference time scale, the sound crossing time in a standard accretion disk between these radii are estimated for Fairall 9 and NGC 5548 by adopting $a_* = 0.998$. The estimated results are listed in column (6) of Table 3. The minus signs of values in column (6) mean that the variations at outer radii lead the variations at inner radii. It can be seen from columns (4) and (6) of Table 3 that the measured time lags are much smaller than those predicted by the standard accretion disks in the case of accretion flow fluctuations travelling inwards.

5. DISCUSSIONS AND CONCLUSIONS

One way of attempting to help testing the standard accretion disk models is to find relationships between variability and fundamental parameters of AGNs, such as black hole mass. The discovery of such a relationship – or lack thereof – may provide useful clues to the physical mechanisms behind the variability. Different sources of optical variations can be associated with different characteristic time scales, and many of these time scales depend on black hole mass. Wold et al. (2007) investigate the dependence of quasar variability on black hole mass, and find that the measured variability amplitude correlates with black hole mass. Collier & Peterson (2001) attempted to define a relationship between black hole mass and characteristic variability time scale. They reported evidence of black hole masses correlating with characteristic optical variability time scales for a sample of 10 well-monitored AGNs. In this paper, a linear correlation between the measured time scales of optical variations and the black hole masses is found for a sample of 26 well-monitored AGNs by reverberation mapping. This linear correlation supports suggestion of Collier & Peterson (2001). The slope of this correlation in equation (15) is ~ 0.12 , and this slope is consistent with the one of ~ 0.15 predicted by equation (3) with the viscosity parameter $\alpha = 0.1$ and the emitting radius $r_d = 100 r_g$. The slopes between the thermal time scale and the black hole mass are estimated for another two emitting radii of $r_d = 50 r_g$ and $r_d = 200 r_g$ in equation (3) with $\alpha = 0.1$. The three theoretical lines between time scales and black hole masses are presented in Figure 6*b*. It can be seen in Figure 6*b* that the theoretical line of $r_d = 100 r_g$ matches the observed data points and the best fit line better than the other two lines do. This means that the measured characteristic time scales of optical variations are likely to be from the accretion disk thermal instability. Then the standard accretion disk models are likely to be conditionally favored by observations.

Another way of attempting to help testing the standard accretion disk models is connect the observed variability time scale with one of the physical time scales in equations (1)–(4). Among the four physical time scales, the thermal time scale is most close to the measured

optical variability time scale as $\alpha = 0.1$. The viscosity parameter α has the typical value of ~ 0.1 for the standard accretion disks (Shakura & Sunyaev 1973). A value of $\alpha \lesssim 1/2$ is implied by the condition that the turbulence should be subsonic in the standard disks (Merloni 2003). A lower value of $\alpha < 0.14$ is suggested by numerical investigations for thin accretion disks with a constant effective speed of sound (Afshordi & Paczynski 2003). Merloni & Nayakshin (2006) also limited a similar range of $\alpha \lesssim 0.15$ on the basis of studying the limit-cycle instability in magnetized accretion disks. Khajenabi & Shadmehri (2007) adopted $\alpha \sim 0.03\text{--}0.3$ to study the dynamical structure of a self-gravitating disk. Then the viscosity parameter α in the standard disks possibly has a wide range including the typical value of $\alpha \sim 0.1$. If the viscosity parameter α is allowed to range from ~ 0.03 to ~ 0.2 , the time scales of optical variations are consistent with the thermal time scales predicted by the standard accretion disk models. This implies that the measured characteristic time scales of optical variations are likely to be produced by the accretion disk thermal instability.

The analysis shows that the wavelength differences $\Delta\lambda$ are correlated with the relevant time lags between different bands for NGC 7469, but there is no correlation between the two quantities for NGC 5548. If the flux variations are caused by the accretion flow fluctuations travelling inwards across the emitting regions, it is likely that the shorter wavelength variations lag the longer wavelength variations. However, the longer wavelength variations lag the shorter wavelength variations for NGC 4151 and NGC 7469. The shorter wavelength variations lag the longer wavelength variations for NGC 5548 except that the variations at 2787 Å lag those at 1841 Å. The variations at 1390 Å lag those at 1880 Å for Fairall 9. If the optical/UV fluxes are the reprocessed continuum with harder photons from the center of accretion disk and softer ones at radii farther out, it is expected that the longer wavelength variations lag the shorter wavelength variations. However, the longer wavelength variations lead the shorter wavelength variations for NGC 5548 and Fairall 9, and this is inconsistent with the expectation in the case of continuum reprocessing. The calculations for NGC 7469 and NGC 4151 show that the time lags estimated in the case of continuum reprocessing are marginally consistent with the measured time lags. In addition, Fairall 9 and NGC 5548 have the black hole mass $M_{\text{BH}} > 5 \times 10^7 M_{\odot}$ with the longer wavelength variations leading the shorter wavelength variations, but NGC 4151 and NGC 7469 have $M_{\text{BH}} < 5 \times 10^7 M_{\odot}$ with the shorter wavelength variations leading the longer wavelength variations (see Table 3). There seems to be a trend between black hole mass and time lag. As black hole mass is above some value, the longer wavelength variations might lead the shorter wavelength variations, but black hole mass is below this value, the shorter wavelength variations might lead the longer wavelength variations.

The origin of the radiation energies emitted in accretion disk is a key to the issue that the harder photons lead or lag the softer ones. For non-blazar type objects, if the optical/UV ra-

diations are the reprocessed X-rays that are commonly attributed to Compton up-scattering of thermal UV seed photons by hot electrons in a corona (e.g., Sunyaev & Titarchuk 1980; Haardt & Maraschi 1991), the optical/UV and X-ray light curves are expected to be correlated with the X-rays leading the optical/UV radiation, and then the harder and softer photons in optical–UV regime are correlated with the harder photons leading the softer ones. The optical/UV emissions in NGC 7469 and NGC 4151 probably belong to this case. If the bulk of the observed optical/UV continuum arises from the viscous dissipation in accretion disk, the resulting light curves would be correlated but the UV radiations should lead the X-rays. This scenario is supported by observations of the Seyfert galaxy MCG–6-30-15 (Arévalo et al. 2005). In this scenario, the observed UV and the seed-photon-emitting regions are connected by perturbations of the accretion flow travelling inwards through the accretion disk, affecting first the main UV emitting radii and then the innermost region where the bulk of the seed photons is expected to be produced (e.g., Arévalo et al. 2005). We analyzed the flux variations in 1–2 KeV (Leighly et al. 1997) and 1855 Å (O’Brien et al. 1998) for 3C 390.3, and a similar behavior to MCG–6-30-15 is found. The time lag estimated by the ZDCF centroid for 3C 390.3 is $\tau_{\text{cent}}^{\text{ob}} = -4.01_{+0.77}^{-1.28}$ days with the X-rays lagging the UV radiation. The UV radiation emitted by NGC 5548 and Fairall 9 might belong to the thermal radiation from the viscous dissipation, and perturbations of the accretion flow travelling inwards through the accretion disk result in the softer photons leading the harder ones. Our results may support that the signs of time lags differ from case to case (e.g., Maoz et al. 2002). The existences of negative as well as positive time lags imply that different processes could be dominating the emissions at different cases, and generally don’t indicate any simple relation between the energy bands.

In this paper, a sample of 26 objects well observed for reverberation mapping is used to test the standard accretion disk models accepted widely by comparing the theoretical expectations to the measured time scales of optical variations, the observed relation of the black hole masses with the measured time scales, and the measured time lags between the optical/UV bands. The time scales measured by both the most common definition of the variability time scale and the zero-crossing time of the ACF are consistent with each other (see Fig. 1). The observed variability time scales are linearly correlated with the black hole masses (see Fig. 6), and this linear relation is conditionally consistent with expectation for the thermal time scales and the black hole masses in equation (3). Adopting the viscosity parameter typically of $\alpha \sim 0.1$ (Shakura & Sunyaev 1973), the thermal time scales are most close to the measured time scales of optical variations. The combinations of $\alpha \sim 0.03$ –0.2 and $a_* = 0.5$ –0.998 could result in the thermal time scales that are in well agreement with the optical variability time scales presented in Table 2. Then it is likely that the optical variations result from the accretion disk thermal instability. The time lags are measured by

the ZDCF method for four ones out of these 26 objects. The analyzed results show that the harder and softer photons at the optical/UV bands are correlated with the harder photons leading the softer ones for NGC 4151 and NGC 7469, and with the harder photons lagging the softer ones for NGC 5548 and Fairall 9 (see Table 3). For NGC 7469 and NGC 4151, the measured time lags are marginally consistent with the time lags estimated in the case of continuum thermal reprocessing. It is possible that the optical/UV emissions of NGC 4151 and NGC 7469 are the reprocessed X-rays that are commonly attributed to Compton up-scattering of thermal UV seed photons by hot electrons. For NGC 5548 and Fairall 9, the UV photons are unlikely to be from the continuum thermal reprocessing in the accretion disk. Our investigations on the variability time scales, the relation of the variability time scales with the black hole masses, and the time lags between different bands are unlikely to be inconsistent with or are likely to be conditionally in favor of the standard accretion disk models of AGNs.

We are grateful to the anonymous referee for his/her constructive comments and suggestions leading to significant improvement of this paper. We are also grateful to Prof. S. Kaspi for his constructive comments and suggestions that helped to significantly improve this paper. Prof. T. Alexander is thanked for kindly providing his ZDCF code. HTL thanks for financial support by National Natural Science Foundation of China (Grant 10778702). JMB is supported by NSFC (Grant 10573030) and (Grant 10778726).

REFERENCES

- Afshordi, N., & Paczynski, B. 2003, *ApJ*, 592, 354
- Alexander, T. 1997, in *Astronomical Time Series*, ed. D. Maoz, A. Sternberg, & E. M. Leibowitz (Dordrecht: Kluwer), 163
- Arévalo, P., Papadakis, I., Kuhlbrodt, B., & Brinkmann, W. 2005, *A&A*, 430, 435
- Aschenbach, B., Grosso, N., Porquet, D., & Predehl, P. 2004, *A&A*, 417, 71
- Bardeen, J. M., Press, W. H., & Teukolsky, S. A. 1972, *ApJ*, 178, 347
- Brenneman, L. W., & Reynolds, C. S. 2006, *ApJ*, 652, 1028
- Carone, T. E., et al. 1996, *ApJ*, 471, 737
- Collier, S. J., et al. 1998, *ApJ*, 500, 162
- Collier, S., & Peterson, B. M. 2001, *ApJ*, 555, 775
- Crenshaw, D. M., et al. 1996, *ApJ*, 470, 322

- Dietrich, M., et al. 1998, *ApJS*, 115, 185
- Ebisawa, K., Mitsuda, K., & Hanawa, T. 1991, *ApJ*, 367, 213
- Edelson, R. A., & Krolik, J. H. 1988, *ApJ*, 333, 646
- Edelson, R. A., et al. 1996, *ApJ*, 470, 364
- Frank, J., King, A., & Raine, D. J. 2002, *Accretion Power in Astrophysics* (Cambridge: Cambridge Univ. Press)
- Gammie, C. F., Shapiro, S. L., & McKinney, J. C. 2004, *ApJ*, 602, 312
- Gaskell, C. M., & Peterson, B. M. 1987, *ApJS*, 65, 1
- Giveon, U., et al. 1999, *MNRAS*, 306, 637
- Haardt, F., & Maraschi, L. 1991, *ApJ*, 380, 51
- Hanawa, T. 1989, *ApJ*, 341, 948
- Isobe, T., Feigelson, E. D., Akritas, M. G., & Babu, G. J. *ApJ*, 1990, 364, 104
- Kaspi, S., et al. 1996, *ApJ*, 470, 336
- Kaspi, S., et al. 2000, *ApJ*, 533, 631
- Kaspi, S., Maoz, D., Netzer, H., Peterson, B. M., Vestergaard, M., & Jannuzi, B. T. 2005, *ApJ*, 629, 61
- Kembhavi, A. K., & Narlika, J. V 1999, *Quasars and Active Galactic Nuclei: An introduction* (Cambridge: Cambridge Univ. Press), p107
- Khajenabi, F., & Shadmehri, M. 2007, *MNRAS*, 377, 1689
- Kriss, G. A., Peterson, B. M., Crenshaw, D. M., & Zheng, W. 2000, *ApJ*, 535, 58
- Krolik, J. H. 1999, *Active Galactic Nuclei: From the Central Black Hole to the Galactic Environment* (Princeton: Princeton Univ. Press), p151–155
- Krolik, J. H., Hawley, J. F., & Hirose, S. 2005, *ApJ*, 622, 1008
- Kubota, A., Ebisawa, K., Makishima, K., & Nakazawa, K. 2005, *ApJ*, 631, 1062
- Leighly, K. M., O’Brien, P. T., Edelson, R., George, I. M., Malkan, M. A., Matsuoka, M., Mushotzky, R. F., & Peterson, B. M. 1997, *ApJ*. 483, 767
- Li, L. X., Zimmerman, E. R., Narayan, R., & McClintock, J. E. 2005, *ApJS*, 157, 335
- Maoz, D., Markowitz, A., Edelson, R., & Nandra, K. 2002, *AJ*, 124, 1988
- McLure, R. J., & Dunlop, J. S. 2004, *MNRAS*, 352, 1390
- Meier, D. L. 2001, *ApJL*, 548, 9

- Meier, D. L. 2002, *New Astronomy Reviews*, 46, 247
- Merloni, A. 2003, *MNRAS*, 2003, 341, 1051
- Merloni, A., & Nayakshin, S. 2006, *MNRAS*, 372, 728
- Netzer, H., et al. 1996, *MNRAS*, 279, 429
- Netzer, H., & Peterson, B. M. 1997, *Astronomical Time Series: Reverberation Mapping and the Physics of Active Galactic Nuclei*, ed. D. Maoz, A. Sternberg, & E. M. Leibowitz (Dordrecht: Kluwer), p85
- O’Brien, P. T., et al. 1998, *ApJ*, 509, 163
- Pariev, V. I., Blackman, E. G., & Boldyrev, S. A. 2003, *A&A*, 407, 403
- Pereyra, N. A., Berk, D. E. V., Turnshek, D. A., & Hillier, D. J. 2006, *ApJ*, 642, 87
- Peterson, B. M., et al. 2000, *ApJ*, 542, 161
- Peterson, B. M., et al. 2004, *ApJ*, 613, 682
- Peterson, B. M., et al. 2005, *ApJ*, 632, 799
- Rees, M. J., Begelman, M. C., Blandford, R. D., & Phinney, E. S. 1982, *Nature*, 295, 17
- Rees, M. J. 1984, *ARA&A*, 22, 471
- Reynolds, C. S., & Nowak, M. A. 2003, *Physics Reports*, 377, 389
- Rodriguez-Pascual, P. M., et al. 1997, *ApJS*, 110, 9
- Roy, M., Papadakis, I. E., Ramos-Colon, E., Sambruna, R., Tsinganos, K., Papamastorakis, J., & Kafatos, M. 2000, *ApJ*, 545, 758
- Santos-Lleo, M., et al. 1997, *ApJS*, 112, 271
- Santos-Lleo, M. et al., 2001, *A&A*, 369, 57
- Shakura, N. I., & Sunyaev, R. A. 1973, *A&A*, 24, 337
- Stirpe, G. M., et al. 1994, *ApJ*, 425, 609
- Sunyaev, R., & Titarchuck, L. G. 1980, *A&A*, 86, 121
- Thorne, K. S. 1974, *ApJ*, 191, 507
- Trevese, D., Kron, R. G., Majewski, S. R., Bershad, M. A., & Koo, D. C. 1994, *ApJ*, 433, 494
- Ulrich, M. H., Maraschi, L., & Urry, C. M. 1997, *ARA&A*, 35, 445
- Urry, C. M., & Padovani, P. 1995, *PASP*, 107, 803
- Vestergaard, M. 2004, *ApJ*, 601, 676

- Vestergaard, M., & Peterson, B. M. 2006, *ApJ*, 641, 689
- Wagner, S. J., & Witzel, A. 1995, *ARA&A*, 33, 163
- Wanders, I., & Peterson, B. M. 1996, *ApJ*, 466, 174
- Wold, M., Brotherton, M. S., & Shang, Z. H. 2007, *MNRAS*, 375, 989
- Woo, J. H., & Urry, C. M. 2002, *ApJ*, 579, 530
- Zimmerman, E. R., Narayan, R., McClintock, J. E., & Miller, J. M. 2005, *ApJ*, 618, 832

Table 1. Sample and data

Objects (1)	z (2)	$\lambda(\text{\AA})$ (3)	Refs. (4)	$\frac{M_{\text{BH}}}{10^8 M_{\odot}}$ (5)	$\frac{L_{\text{bol}}}{\text{ergs s}^{-1}}$ (6)
PG 0026+129	0.142	5100	1, 2	3.93	45.39
PG 0052+251	0.155	5100	1, 2	3.69	45.93
Fairall 9	0.047	5340	3	2.55	45.23
		1880	4		
		1390	4		
PG 0804+761	0.100	5100	1, 2	6.93	45.93
PG 0844+349	0.064	5100	1, 2	9.24	45.36
PG 0953+414	0.239	5100	1, 2	2.76	46.16
NGC 3783	0.010	5150	5	0.30	44.41
NGC 4051	0.002	5100	6	0.02	43.56
NGC 4151	0.003	5125	7	0.13	43.73
		2688	8		
		1440	8		
		1275	8		
PG 1211+143	0.085	5100	1, 2	1.46	45.81
PG 1226+023	0.158	5100	1, 2	8.86	47.35
PG 1229+204	0.064	5100	1, 2	0.73	45.01
PG 1307+085	0.155	5100	1, 2	4.40	45.83
Mrk 279	0.030	5100	9	0.35	44.83
PG 1351+640	0.087	5100	1, 2	0.46	45.50
PG 1411+442	0.089	5100	1, 2	4.43	45.58
NGC 5548	0.017	5150	10	0.67	44.83
		2787	11		
		2441	11		
		2237	11		
		1841	11		
		1749	11		
		1378	11		
PG 1426+015	0.086	5100	1, 2	12.98	45.19
PG 1613+658	0.129	5100	1, 2	2.79	45.66

Table 1—Continued

Objects (1)	z (2)	$\lambda(\text{\AA})$ (3)	Refs. (4)	$\frac{M_{\text{BH}}}{10^8 M_{\odot}}$ (5)	$\frac{L_{\text{bol}}}{\text{ergs s}^{-1}}$ (6)
PG 1617+175	0.114	5100	1, 2	5.94	45.22
PG 1700+518	0.292	5100	1, 2	7.81	46.56
PG 1704+608	0.371	5100	1, 2	0.37	46.33
3C 390.3	0.056	5177	12	2.87	44.88
Mrk 509	0.034	5100	13	1.43	45.03
PG 2130+099	0.061	5100	1, 2	4.57	45.47
NGC 7469	0.016	4845	14	0.12	45.28
		6962	14		
		1825	15		
		1740	15		
		1485	15		
		1315	15		

Note. — Col: (1) name. Col: (2) redshift. Col: (3) the rest frame wavelengths of light curves. Col: (4) the references of light curves. Col: (5) black hole mass. Col: (6) log of the bolometric luminosity.

References. — (1) Kaspi et al. 2000; (2) Kaspi et al. 2005; (3) Santos-Lleo et al. 1997; (4) Rodriguez-Pascual et al. 1997; (5) Stirpe et al. 1994; (6) Peterson et al. 2000; (7) Kaspi et al. 1996; (8) Crenshaw et al. 1996; (9) Santos-Lleo et al. 2001; (10) Wanders & Peterson 1996; (11) the UltraViolet Light Curve Database for AGNs; (12) Dietrich et al. 1998; (13) Carone et al. 1996; (14) Collier et al. 1998; (15) Kriss et al. 2000.

Table 2. Calculated results

Objects (1)	$\frac{\tau/(1+z)}{\text{days}}$ (2)	$\frac{\tau_0/(1+z)}{\text{days}}$ (3)	$\frac{\tau_1}{\text{days}}$ (4)	$\frac{\tau_{\text{dyn}}}{\text{days}}$ (5)	$\frac{\tau_{\text{th}}}{\text{days}}$ (6)	$\frac{\tau_{\text{s}}}{\text{days}}$ (7)
PG 0026	343.6 ± 1.6	$182.7_{+9.2}^{-3.5}$	1.20	8.22	84.01	$2.14 \cdot 10^4$
			1.02	6.39	65.74	$1.82 \cdot 10^4$
			0.99	6.08	62.09	$1.78 \cdot 10^4$
			0.79	4.26	43.83	$1.41 \cdot 10^4$
PG 0052	242.5 ± 1.8	$326.4_{+10.5}^{-6.4}$	1.85	16.44	164.36	$3.31 \cdot 10^4$
			1.64	13.70	135.14	$2.94 \cdot 10^4$
			1.52	12.18	120.53	$2.72 \cdot 10^4$
			1.20	8.52	84.01	$2.15 \cdot 10^4$
Fairall 9	160.8 ± 0.3	$110.6_{+8.8}^{-2.6}$	1.00	7.91	76.70	$1.83 \cdot 10^4$
			0.89	6.39	65.75	$1.62 \cdot 10^4$
			0.82	5.78	58.44	$1.51 \cdot 10^4$
			0.65	3.96	40.18	$1.19 \cdot 10^4$
PG 0804	385.5 ± 0.7	$497.0_{+7.2}^{-5.7}$	2.20	15.52	153.41	$3.93 \cdot 10^4$
			1.97	13.09	131.49	$3.52 \cdot 10^4$
			1.83	11.57	116.88	$3.27 \cdot 10^4$
			1.45	8.22	84.01	$2.59 \cdot 10^4$
PG 0844	313.1 ± 1.3	$134.8_{+9.0}^{-5.3}$	1.44	7.00	69.40	$2.57 \cdot 10^4$
			1.31	6.09	62.09	$2.34 \cdot 10^4$
			1.23	5.48	54.79	$2.19 \cdot 10^4$
			0.99	3.96	40.18	$1.76 \cdot 10^4$
PG 0953	275.1 ± 0.7	$772.0_{+6.3}^{-5.2}$	2.05	21.92	219.15	$3.67 \cdot 10^4$
			1.82	18.26	182.63	$3.25 \cdot 10^4$
			1.68	16.44	164.36	$3.01 \cdot 10^4$
			1.35	11.57	113.23	$2.37 \cdot 10^4$
NGC 3783	38.2 ± 2.8	$29.5_{+0.20}^{-0.14}$	0.26	3.04	29.22	$4.69 \cdot 10^3$
			0.23	2.44	25.57	$4.15 \cdot 10^3$
			0.21	2.13	21.92	$3.84 \cdot 10^3$
			0.17	1.52	14.61	$3.02 \cdot 10^3$
NGC 4051	120.3 ± 0.05	$165.4_{+0.30}^{-0.40}$	0.06	1.22	10.96	$1.02 \cdot 10^3$
			0.05	0.91	10.96	$8.99 \cdot 10^2$

Table 2—Continued

Objects (1)	$\frac{\tau/(1+z)}{\text{days}}$ (2)	$\frac{\tau_0/(1+z)}{\text{days}}$ (3)	$\frac{\tau_1}{\text{days}}$ (4)	$\frac{\tau_{\text{dyn}}}{\text{days}}$ (5)	$\frac{\tau_{\text{th}}}{\text{days}}$ (6)	$\frac{\tau_{\text{s}}}{\text{days}}$ (7)
			0.05	0.91	7.31	$8.29 \cdot 10^2$
			0.04	0.61	7.31	$6.50 \cdot 10^2$
NGC 4151	70.4 ± 0.6	$45.0_{+0.13}^{-0.20}$	0.12	1.52	14.61	$2.10 \cdot 10^3$
			0.10	1.22	10.96	$1.85 \cdot 10^3$
			0.09	0.91	10.96	$1.71 \cdot 10^3$
			0.08	0.61	7.31	$1.35 \cdot 10^3$
PG 1211	237.1 ± 0.8	$533.4_{+11.9}^{-3.8}$	1.28	14.91	149.75	$2.29 \cdot 10^4$
			1.13	12.48	124.19	$2.03 \cdot 10^4$
			1.05	10.96	109.58	$1.87 \cdot 10^4$
			0.83	7.61	76.70	$1.47 \cdot 10^4$
PG 1226	314.4 ± 5.7	$401.2_{+5.5}^{-2.6}$	7.61	87.66	876.60	$1.36 \cdot 10^5$
			6.72	72.75	726.85	$1.20 \cdot 10^5$
			6.23	64.83	650.15	$1.11 \cdot 10^5$
			4.90	45.35	452.91	$8.77 \cdot 10^4$
PG 1229	124.5 ± 4.3	$143.0_{+2.8}^{-2.2}$	0.55	5.78	58.44	$9.76 \cdot 10^3$
			0.48	4.87	47.48	$8.62 \cdot 10^3$
			0.44	4.26	40.18	$7.99 \cdot 10^3$
			0.35	3.04	29.22	$6.30 \cdot 10^3$
PG 1307	234.2 ± 7.7	$294.8_{+4.3}^{-3.6}$	1.79	14.31	142.45	$3.20 \cdot 10^4$
			1.59	11.87	120.53	$2.84 \cdot 10^4$
			1.48	10.65	105.92	$2.64 \cdot 10^4$
			1.17	7.61	76.70	$2.09 \cdot 10^4$
Mrk 279	86.5 ± 2.9	$76.5_{+0.91}^{-0.15}$	0.38	4.87	47.48	$6.78 \cdot 10^3$
			0.33	3.96	40.18	$5.98 \cdot 10^3$
			0.31	3.65	36.53	$5.53 \cdot 10^3$
			0.24	2.44	25.57	$4.35 \cdot 10^3$
PG 1351	423.6 ± 1.7	$476.4_{+4.9}^{-2.8}$	0.70	10.96	109.58	$1.26 \cdot 10^4$
			0.62	9.13	91.31	$1.11 \cdot 10^4$
			0.57	7.91	76.70	$1.02 \cdot 10^4$
			0.45	5.48	54.79	$8.07 \cdot 10^3$

Table 2—Continued

Objects (1)	$\frac{\tau/(1+z)}{\text{days}}$ (2)	$\frac{\tau_0/(1+z)}{\text{days}}$ (3)	$\frac{\tau_1}{\text{days}}$ (4)	$\frac{\tau_{\text{dyn}}}{\text{days}}$ (5)	$\frac{\tau_{\text{th}}}{\text{days}}$ (6)	$\frac{\tau_{\text{s}}}{\text{days}}$ (7)
PG 1411	317.4 ± 1.4	$356.6_{+4.1}^{-2.3}$	1.45	10.35	102.27	$2.60 \cdot 10^4$
			1.30	8.83	87.66	$2.32 \cdot 10^4$
			1.20	7.61	76.70	$2.16 \cdot 10^4$
			0.96	5.48	54.79	$1.71 \cdot 10^4$
NGC 5548	45.1 ± 1.1	$141.5_{+7.1}^{-2.8}$	0.47	4.87	47.48	$8.36 \cdot 10^3$
			0.41	3.96	40.18	$7.37 \cdot 10^3$
			0.38	3.35	36.53	$6.86 \cdot 10^3$
			0.30	2.44	25.57	$5.38 \cdot 10^3$
PG 1426	638.7 ± 1.9	$852.0_{+20.2}^{-18.0}$	1.30	5.17	51.14	$2.33 \cdot 10^4$
			1.22	4.57	47.48	$2.17 \cdot 10^4$
			1.15	4.26	43.83	$2.06 \cdot 10^4$
			0.94	3.04	32.87	$1.68 \cdot 10^4$
PG 1613	309.5 ± 1.2	$232.1_{+7.5}^{-4.9}$	1.37	11.87	120.53	$2.45 \cdot 10^4$
			1.22	10.04	98.62	$2.17 \cdot 10^4$
			1.12	8.83	87.66	$2.01 \cdot 10^4$
			0.89	6.39	62.09	$1.59 \cdot 10^4$
PG 1617	277.9 ± 3.6	$187.9_{+6.1}^{-6.3}$	1.15	6.39	62.09	$2.06 \cdot 10^4$
			1.04	5.48	54.79	$1.86 \cdot 10^4$
			0.97	4.87	47.48	$1.73 \cdot 10^4$
			0.77	3.35	36.53	$1.38 \cdot 10^4$
PG 1700	470.4 ± 87.4	$419.3_{+12.2}^{-10.2}$	3.85	33.48	336.03	$6.88 \cdot 10^4$
			3.42	28.00	281.24	$6.11 \cdot 10^4$
			3.17	24.96	252.02	$5.68 \cdot 10^4$
			2.50	17.65	175.32	$4.47 \cdot 10^4$
PG 1704	286.7 ± 5.9	$389.1_{+8.8}^{-7.4}$	1.27	29.22	292.20	$2.27 \cdot 10^4$
			1.12	24.05	241.07	$1.99 \cdot 10^4$
			1.03	21.31	211.85	$1.84 \cdot 10^4$
			0.81	14.91	149.75	$1.45 \cdot 10^4$
3C 390.3	143.8 ± 0.6	$50.6_{+0.63}^{-0.46}$	0.73	4.57	47.48	$1.32 \cdot 10^4$
			0.66	3.96	40.18	$1.23 \cdot 10^4$

Table 2—Continued

Objects (1)	$\frac{\tau/(1+z)}{\text{days}}$ (2)	$\frac{\tau_0/(1+z)}{\text{days}}$ (3)	$\frac{\tau_l}{\text{days}}$ (4)	$\frac{\tau_{\text{dyn}}}{\text{days}}$ (5)	$\frac{\tau_{\text{th}}}{\text{days}}$ (6)	$\frac{\tau_s}{\text{days}}$ (7)
Mrk 509	258.7 ± 1.0	$181.0_{-2.2}^{-1.7}$	0.61	3.35	32.87	$1.10 \cdot 10^4$
			0.49	2.44	25.57	$8.76 \cdot 10^3$
			0.67	5.78	58.44	$1.20 \cdot 10^4$
			0.60	4.87	47.48	$1.07 \cdot 10^4$
			0.55	4.26	40.18	$9.92 \cdot 10^3$
PG 2130	319.0 ± 12.3	$332.9_{+11.0}^{-5.0}$	0.44	3.04	29.22	$7.84 \cdot 10^3$
			1.28	8.52	84.01	$2.28 \cdot 10^4$
			1.20	7.61	76.70	$2.14 \cdot 10^4$
			1.11	6.70	69.40	$1.99 \cdot 10^4$
NGC 7469	74.9 ± 0.8	$4.5_{+0.02}^{-0.05}$	0.88	4.87	47.48	$1.58 \cdot 10^4$
			0.36	7.91	80.36	$6.33 \cdot 10^3$
			0.32	6.39	65.75	$5.56 \cdot 10^3$
			0.29	5.48	54.79	$5.13 \cdot 10^3$
			0.23	4.26	40.18	$4.16 \cdot 10^3$

Note. — Col: (1) name. Col: (2) variability time scale at the optical band. Col: (3) variability time scale obtained by the zero-crossing time of the ACF estimated by the ZDCF. Col: (4) light crossing time scales. Col: (5) dynamical time scales. Col: (6) thermal time scales. Col: (7) sound crossing time scales. For each object, the first, second, third, and fourth values listed in columns (4)–(7) are calculated from the standard accretion disks under the Kerr metric with spin parameter $a_* = 0.5, 0.8, 0.9,$ and $0.998,$ respectively.

Table 3. Time lags

Objects (1)	$\lambda_1(\text{\AA})$ (2)	$\lambda_2(\text{\AA})$ (3)	$\tau_{\text{cent}}^{\text{ob}}$ (days) (4) ^a	τ_{rep} (days) (5) ^a	τ_{lag} (yrs) (6) ^a
Fairall 9	1390	1880	$-3.71_{+0.68}^{-0.66}$	^b 0.08 0.07 0.05	-1.95
NGC 4151	1440	2688	$0.17_{+0.08}^{-0.01}$	0.03 0.02 0.02 0.02	-0.75
	1275	2688	$0.09_{+0.08}^{-0.01}$	0.03 0.03 0.03 0.02	-0.82
NGC 5548	1841	2787	$0.72_{+0.18}^{-0.16}$	0.09 0.08 0.07 0.06	-2.52
	1841	2441	$-0.54_{+0.17}^{-0.15}$	0.06 0.05 0.04 0.03	-1.49
	1841	2237	$-0.55_{+0.17}^{-0.16}$	0.04 0.03 0.03 0.02	-0.93
	1749	2787	$-0.98_{+0.17}^{-0.11}$	0.10 0.09 0.08 0.06	-2.72
	1749	2441	$-0.67_{+0.21}^{-0.20}$	0.06 0.06 0.05 0.04	-1.69
	1749	2237	$-0.68_{+0.20}^{-0.19}$	0.04 0.04 0.03 0.03	-1.13
	1378	2787	$-0.64_{+0.19}^{-0.18}$	0.13 0.11 0.10 0.08	-3.41
	1378	2441	$-0.61_{+0.19}^{-0.18}$	0.09 0.08 0.07 0.06	-2.39
	1378	2237	$-0.64_{+0.19}^{-0.18}$	0.07 0.06 0.06 0.05	-1.82
	1378	1841	$-1.43_{+0.06}^{-0.05}$	0.04 0.03 0.03 0.02	-0.90
NGC 7469	1825	6962	$0.83_{+0.13}^{-0.04}$	0.50 0.44 0.41 0.32	-19.88
	1740	6962	$1.46_{+0.18}^{-0.08}$	0.51 0.44 0.41 0.32	-20.03
	1485	6962	$1.72_{+0.18}^{-0.08}$	0.52 0.46 0.42 0.33	-20.45
	1315	6962	$1.72_{+0.18}^{-0.08}$	0.53 0.47 0.43 0.34	-20.70
	1825	4845	$0.99_{+0.17}^{-0.08}$	0.27 0.24 0.22 0.17	-9.29
	1740	4845	$0.99_{+0.17}^{-0.08}$	0.28 0.24 0.22 0.18	-9.44
	1485	4845	$1.01_{+0.16}^{-0.07}$	0.29 0.26 0.24 0.19	-9.86
	1315	4845	$1.23_{+0.17}^{-0.08}$	0.30 0.27 0.25 0.19	-10.10
	1315	1825	$0.32_{+0.27}^{-0.19}$	0.03 0.03 0.03 0.02	-0.82

^aThe sign of the time lag is defined as $\tau_{\text{cent,rep,lag}} = t(\lambda_2) - t(\lambda_1)$.

^bIn case of $a_* = 0.5$, the temperature of disk is not high enough to emit radiation at 1390 \AA .

Note. — Col: (1) name. Col: (2) wavelengths of the first light curves.

Col: (3) wavelengths of the second light curves. Col: (4) the observed time lags of the first light curves relative to the second ones. Col: (5) the continuum reprocessing time lags, and the first, second, third, and fourth values are estimated from the standard accretion disks under the Kerr metric with spin parameter $a_* = 0.5, 0.8, 0.9,$ and $0.998,$ respectively. Col: (6) the sound crossing time lags estimated with spin $a_* = 0.998.$

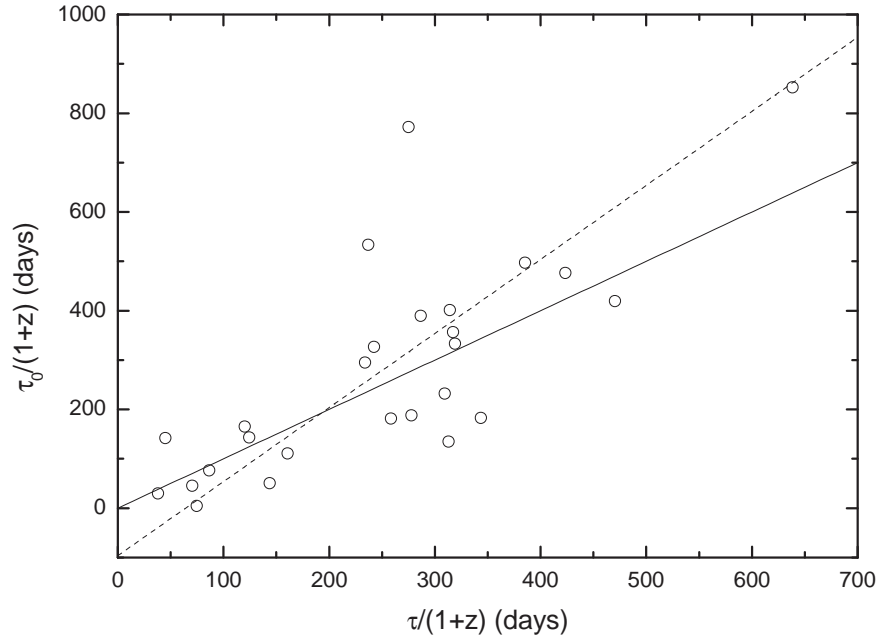


Fig. 1.— The plot of τ_0 vs τ . The solid line presents $\tau_0 = \tau$. The dashed line denotes the best linear fit.

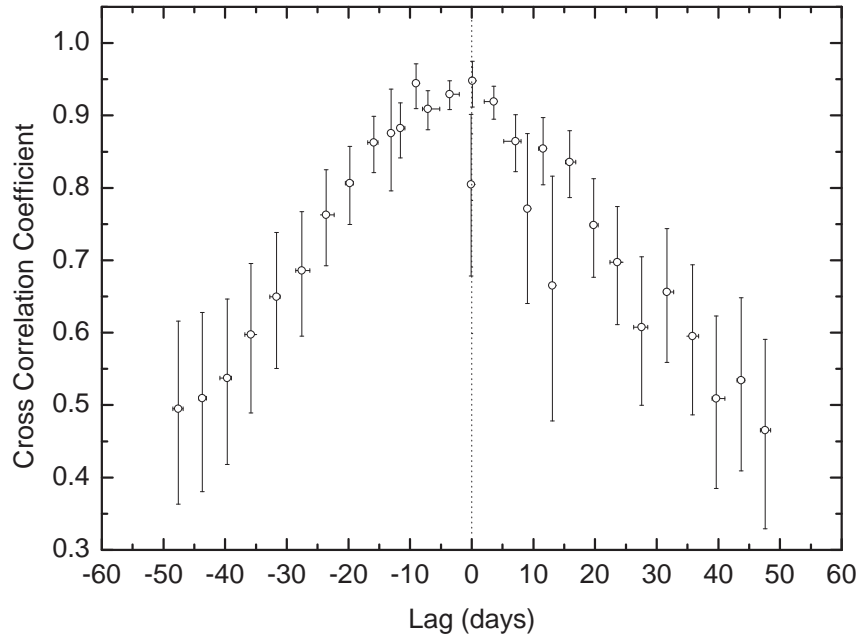


Fig. 2.— ZDCF for Fairall 9 between 1880 Å and 1390 Å light curves.

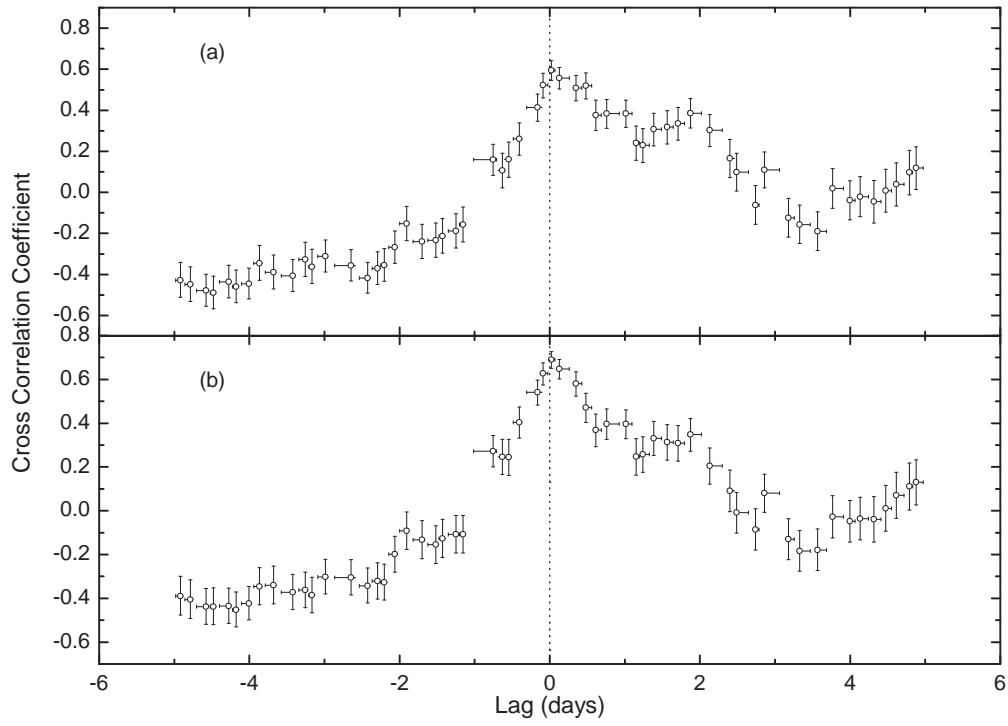


Fig. 3.— ZDCF for NGC 4151. (a) ZDCF between 2688 Å and 1440 Å light curves. (b) ZDCF between 2688 Å and 1275 Å.

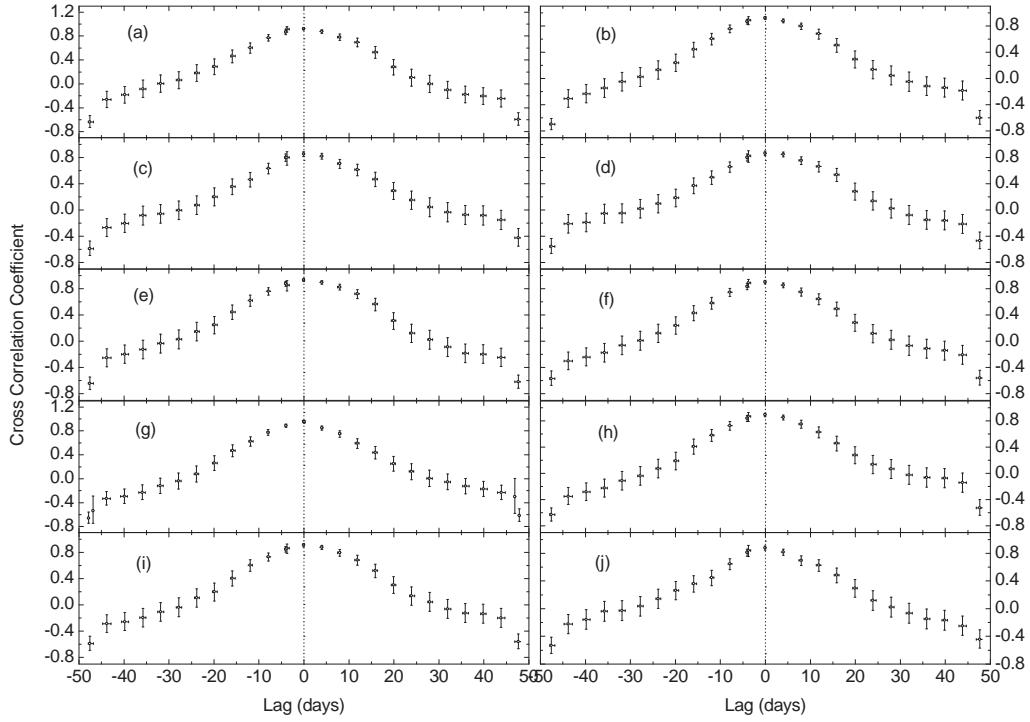
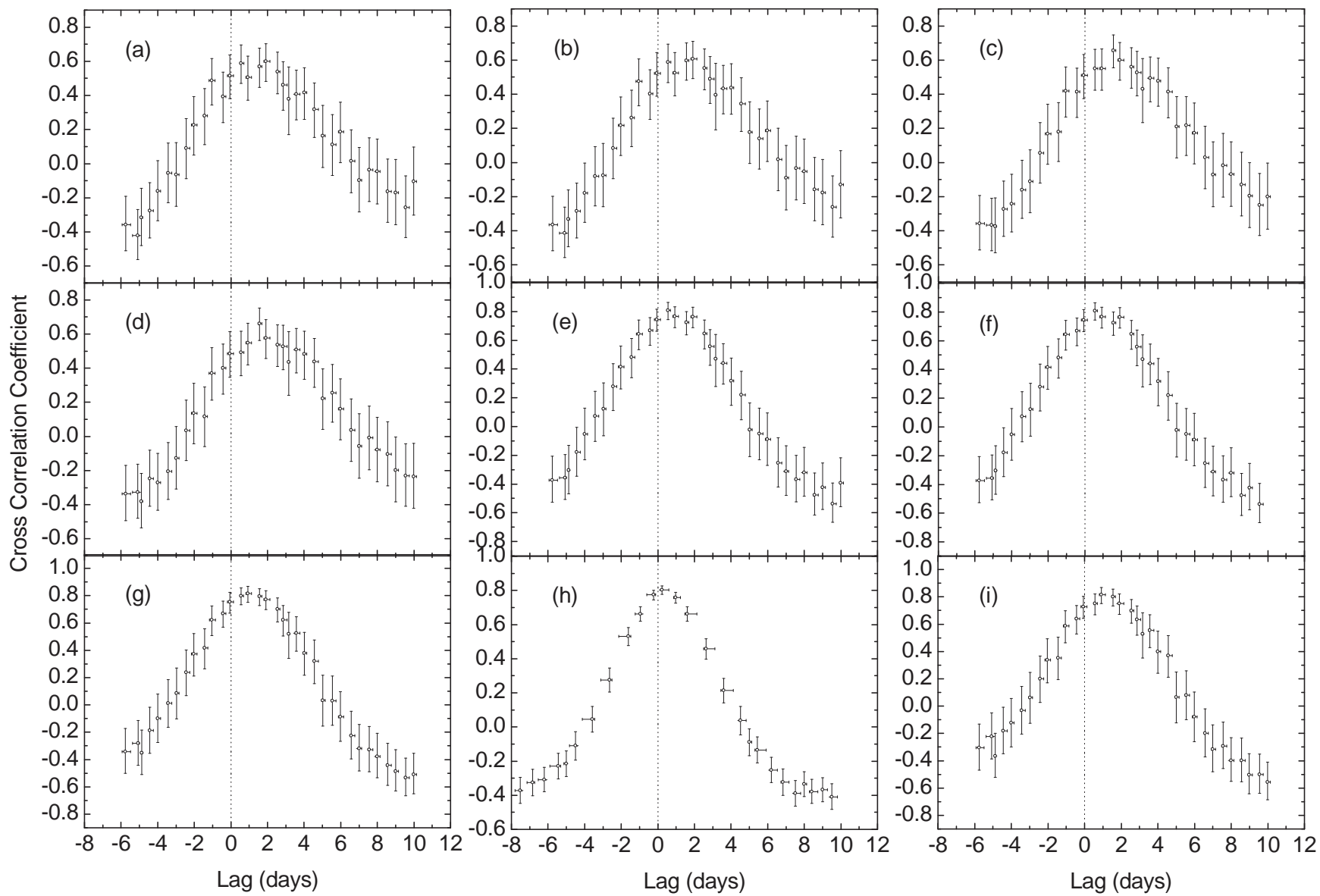


Fig. 4.— ZDCF for NGC 5548. (a) ZDCF between 2441 Å and 1749 Å light curves. (b) ZDCF between 2441 Å and 1378 Å. (c) ZDCF between 2787 Å and 1378 Å. (d) ZDCF between 2787 Å and 1841 Å. (e) ZDCF between 2441 Å and 1841 Å. (f) ZDCF between 2237 Å and 1749 Å. (g) ZDCF between 1841 Å and 1378 Å. (h) ZDCF between 2237 Å and 1378 Å. (i) ZDCF between 2237 Å and 1841 Å. (j) ZDCF between 2787 Å and 1749 Å.



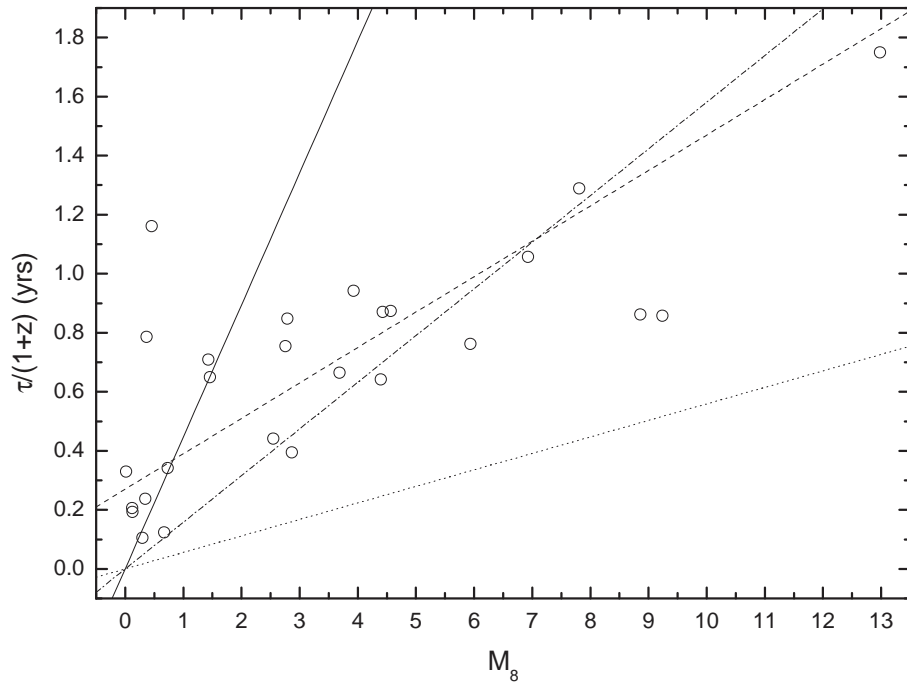


Fig. 6.— The plot of τ vs M_8 . The dashed line denotes the best linear fit. The dotted, dash-dotted, and solid lines are the theoretical lines of equation (3) for $r_d = 50 r_g$, $100 r_g$, and $200 r_g$, respectively.